

Complete band gaps for magnetostatic forward volume waves in a two-dimensional magnonic crystal

T. Schwarze, R. Huber, G. Duerr, and D. Grundler*

*Lehrstuhl für Physik funktionaler Schichtsysteme, Technische Universität München, Physik Department,
James Franck Strasse 1, D-85747 Garching bei München, Germany*

(Received 12 January 2012; published 27 April 2012)

We report on the formation of a complete band gap for spin waves in a two-dimensional magnonic crystal consisting of a periodic hole lattice. We go beyond the partial band gaps observed so far in that we apply a magnetic field perpendicular to the permalloy thin film. We explore the relevant geometrical parameters using micromagnetic simulations. In nanopatterned devices we obtain complete band gaps of up to 1.4 GHz. The magnetostatic forward volume waves addressed here overcome in particular spin-wave localization effects. These effects have led to complicated and highly anisotropic miniband formation or Bragg reflection in in-plane fields for a long time. We demonstrate how direct band-gap tailoring via geometrical lattice symmetries becomes possible in nanostructured magnetic antidot lattices.

DOI: [10.1103/PhysRevB.85.134448](https://doi.org/10.1103/PhysRevB.85.134448)

PACS number(s): 75.40.Gb, 75.30.Ds, 75.75.-c, 75.78.-n

I. INTRODUCTION

Modern information technology relies mainly on the storage, movement, and processing of charge carriers. Here, physical limits in both miniaturization and processing speed might be reached in the near future, therefore further technologies need to be explored to advance current devices.^{1,2} Spin waves in magnetic materials in particular offer advantages for data processing at gigahertz frequencies due to their short wavelength being in the 100 nm range.³ Magnonic devices therefore hold great promise in downscaling microwave devices.⁴ The downscaling argument is similar to surface acoustic wave based gigahertz filters and delay lines which are an integral part of the telecommunications market.⁵ However, spin waves go beyond that in that the functionality can be reprogrammed via the magnetic history.^{6,7} Magnonic crystals (MCs) consisting of a periodic lattice of nanoholes [i.e., the so-called magnetic antidot lattices (ADLs)] have generated in particular great interest.⁸ Such devices are the magnetic analog of photonic crystals making use of air holes in a dielectric layer.⁹ So far the magnetic devices have been investigated almost exclusively in magnetic fields \mathbf{H} applied in the plane of the ferromagnetic thin film being mostly $\text{Ni}_{80}\text{Fe}_{20}$ (permalloy).^{10–24} Allowed minibands and partial band gaps have been observed but only for specific directions of the wave vector k (Refs. 25 and 26). The dispersion relations have been found to depend crucially on \mathbf{H} because the inhomogeneous demagnetization fields created by the holes varied significantly the refractive index of the spin waves in the permalloy thin films.^{18,24} This provoked a spin-wave localization counteracting miniband formation. Nanostructured ADLs and in particular spin-wave propagation therein have been investigated far less in perpendicular magnetic fields.²⁷ Theoretical approaches such as the plane wave method, dynamical matrix method, and micromagnetic simulations have already been shown to model the experimentally observed dispersion relations.^{25,26} Micromagnetic simulations in magnonics^{29,30} offer the perspective to model nonperiodic defects such as missing holes and local lattice constant variations in a more straightforward manner. Such intentional defects have provoked functional photonic crystal devices.⁹ In magnonics, however, the inhomogeneous

demagnetization fields created by the holes are a severe drawback. At the same time, magnetostatic forward volume waves (MSFVWs) are particularly interesting for coherent mode formation in MCs as they exhibit the lowest propagation loss per unit time.^{31,32} In this paper we show that a perpendicular magnetic field applied to a magnetic antidot lattice improves the performance of magnetic antidot lattices considerably. It avoids spin-wave localization. In particular, the allowed minibands and forbidden frequency gaps are formed for the MSFVWs which are less anisotropic compared to the previous studies. This allows us to provoke complete band gaps (stop bands) in the two-dimensional (2D) magnonic device. Such 2D devices go beyond previously published one-dimensional MCs based on the resonant backscattering of spin waves^{33,34} and open intriguing perspectives for the control and manipulation of spin waves.

The paper is organized as follows. In Sec. II A we introduce micromagnetic simulations and outline our simulation geometry and all relevant parameters used throughout this paper. In Sec. II B we present our results obtained from micromagnetic simulations. In Sec. III we discuss our findings on band formation in the two-dimensional magnonic crystals.

II. MICROMAGNETIC SIMULATIONS

A. Simulation geometry and parameters

We consider a periodic array of holes in a permalloy thin film as shown in Fig. 1 and perform micromagnetic simulations for different lattice parameters. In particular we assume an out-of-plane field $\mu_0\mathbf{H}$ of 1.2 T. This is larger than the anisotropy field of a permalloy film of about 1 T and forces the magnetic moments to follow \mathbf{H} . Only close to holes edges magnetic moments are found to be canted (Fig. 1). Wave vectors \mathbf{k} are in the plane (i.e., we address MSFVWs). To get timely and spatially resolved data of the magnetization dynamics we employ micromagnetic simulations using the MICROMAGUS software package which provides us with in particular 2D periodic boundary conditions.³⁵ These are essential to avoid finite-size effects for the array.³⁶ We simulate a stripe of several unit cells extending either in the x direction or a direction

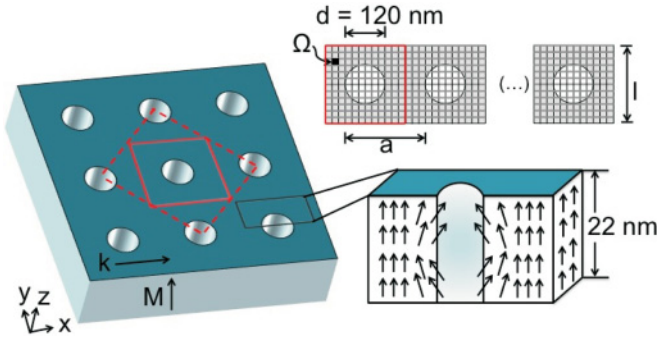


FIG. 1. (Color online) Left: Schematic illustration of the periodic lattice of holes (bright) in a magnetic film (dark). The unit cells for simulations assuming periodic boundary conditions are marked as follows: solid line, in-plane wave vector k is along the primitive lattice vector; broken line, k is along the diagonal of the square lattice. We consider an external field of 1.2 T to be applied in the out-of-plane direction (z direction). The configuration of magnetic moments (arrows) at 1.2 T is taken from a simulation with $\delta = 5.5$ nm and illustrated at the bottom on the right. In the upper right corner we display the parameters varied in the simulations (i.e., the lattice periodicity a and the number of simulation cells $n = l/\Omega$ in the x and y directions).

which has an angle of 45° with the x direction. We use the periodic boundary conditions to address the infinite lattice. The unit cell is discretized into small simulation cells exhibiting a volume of $\Omega = a/n \times a/n \times \delta$, where a is the lattice constant of the ADL and n^2 is the number of simulation cells in the plane. We tested unit cell sizes δ of both 22 and 5.5 nm in the z direction (i.e., one and four cells, respectively, for the 22-nm thick film). The dispersion relations did not depend on δ . The spin waves are excited using a short and localized field pulse of $\mu_0 h_{\text{rf}} = 0.1$ mT directed 45° out of the xy plane and a rise and fall time of 6 ps. The time duration for our simulation is typically 10 ns. The simulation gives us the response in time and space of the local magnetization and after a two-step fast Fourier transformation (FFT) of the simulated in-plane magnetization m_x we obtain the integrated spectral response $P(f, k)$ providing us with the dispersion relation $f(k)$ ²⁹ (f is the frequency). We use the material parameters of permalloy which has turned out to be a material relevant in the field of magnonics. The saturation magnetization is set to 780 kA/m and the exchange constant is 1.3×10^{-11} J/m. We assume a damping parameter $\alpha = 0.005$. No intrinsic magnetic anisotropy is considered in our simulations. In this study the diameter of the holes is kept constant at $d = 120$ nm, whereas the lattice period a is varied.

B. Results

In Fig. 2(a) we show the dispersion relation for a plain film. Here we set the hole diameter in the simulations to zero. We find a single branch (bright) starting at about 6.2 GHz at $k = 0$. This is the MSFVW. For positive k we find a positive slope reflecting a group velocity $v_g = 2\pi \partial f / \partial k$ of 0.9 km/s (Ref. 37). Along the branch data points are missing in specific regions of k which are in particular periodic as a function of k . Such regions are artefacts from the numerical simulations due to the finite length of the stripe in x direction and the corresponding

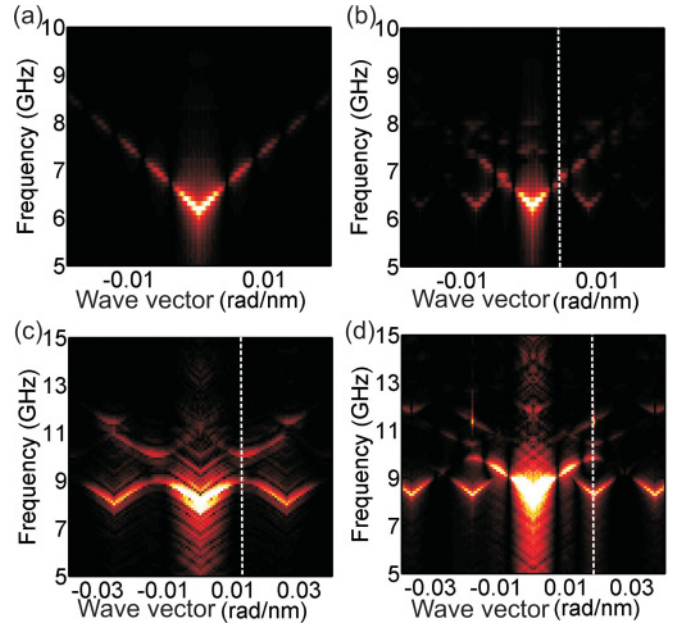


FIG. 2. (Color online) Color coded spin-wave dispersion for (a) plain film, (b) ADL with $a = 800$ nm and (c) ADL with $a = 240$ nm when k is pointing along a primitive vector, and (d) 45° deg-rotated k pointing along the diagonal of an ADL with $a = 240$ nm. Here dark color means no spin-wave excitation and bright means high spin-wave excitation. In (b), (c) and (d) the first BZ is indicated by the white dashed line. Note that due to the discretization of the holes edges being periodic from unit cell to unit additional spin waves are faintly excited. In a real device we do not expect to observe such features as the edge roughness over the MC would be irregular.

periodic boundary condition. They do not reflect a forbidden frequency gap in the magnetic device. The branch is expected to be continuous in such regions of k . The faintly bright regions around $k = 0$ are attributed to numerical artefacts coming from the discretization in real space due to the finite-sized simulation cells. In the simulations of the ADLs the artefacts will partly be even more pronounced. For the discussion we will focus on regimes of the wave vector k where artefacts do not play a role.

In Fig. 2(b) we show the simulated dispersion of an ADL with a periodicity of $a = 800$ nm. The wave vector is oriented in the x direction. Starting from about 6.2 GHz a branch is seen for positive k which has a slope similar to the branch observed for the unpatterned film. In the patterned device, however, there are further excitations at about 6.2 GHz positioned at negative and positive wave vectors k . Analyzing their absolute values we find that they correspond to the reciprocal lattice vector $|\mathbf{G}| = 2\pi/a$. The band structure has become periodic in reciprocal space. Figure 2 thus displays the dispersion relation in the so-called extended zone scheme where k extends beyond the first Brillouin zone (BZ) boundary located at $k_{\text{BZb}} = \pi/a$ (vertical broken line). At this point the resolution of the data is not large enough to decide whether there is a crossing or avoided crossing (anticrossing) of the different branches at the first BZ boundary. The simulations predict further faint modes at high frequencies which we do not address here.

In Fig. 2(c) we depict the dispersion relation for $a = 240$ nm. Correspondingly, the Brillouin zone boundary resides at a larger absolute value $k_{\text{BZb}} = \pi/a$ (indicated by the vertical

broken line). Two prominent branches are seen at $k_{\text{BZb}} = \pi/a$ that are separated by a forbidden frequency gap [i.e., a band gap (stop band) with a width of about 1.2 GHz between 8.9 and 10.1 GHz]. The additional resonances can be viewed as backfolded branches of the unpatterned film. At $k_{\text{BZb}} = \pi/a$ the branches which anticross exhibit a group velocity $v_g = 0$ reflecting standing spin waves at a finite k . The gap of 1.2 GHz is formed for k being collinear to the primitive lattice vector in the x direction of the assumed square lattice. Due to the specific perpendicular-to-plane direction of \mathbf{H} the dispersion relation $f(k)$ and forbidden frequency gaps are the same for the two different in-plane directions x and y . This is different from previous investigations on antidot lattices in in-plane fields.^{10–24} We note that the bright regions near $k = 0$ in Fig. 2(c) are more pronounced compared to Fig. 2(a). We attribute this to the roughness of the holes introduced via the finite-sized simulation cells. The cells are square-shaped such that the hole edges are not smooth. In the short-period hole lattice of Fig. 2(c) where a is only twice the hole diameter the edge roughness is effective to excite spin waves with a broad distribution of wave vectors. As a consequence, the effective linewidth is much broader than given by the damping parameter α (Ref. 38).

It is interesting to study the width of the band gap for different lattice constants. For this we consider \mathbf{k} pointing along the primitive lattice vector and vary a in discrete steps between 180 and 800 nm. The extracted eigenfrequencies at BZ boundaries (symbols) are summarized in Fig. 3(a). The colored (white) regions highlight forbidden frequency regions (allowed minibands) as interpolated from the discrete dataset as a function of a . For the solid lines we assume exponential fitting functions following a phenomenological approach as

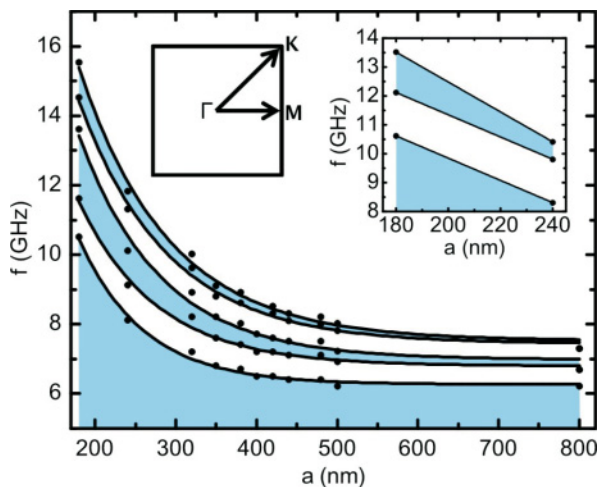


FIG. 3. (Color online) (a) Symbols denote eigenfrequencies at BZ boundaries for ADLs with different lattice constants a and \mathbf{k} pointing along the ΓM direction (see inset). The colored regions indicate the forbidden frequency regions evaluated from the simulations. The white areas limited by blue regions denote the widths of the allowed minibands. The straight lines are guides to the eyes obtained by fitting exponential functions. (b) Eigenfrequencies at BZ boundaries (symbol) for ADLs with different lattice constants a and \mathbf{k} pointing along ΓK direction (i.e., under 45°). The colored regions indicate the forbidden frequency regions evaluated from the simulations. Straight lines are guides to the eyes.

will be discussed later. The fitting functions extrapolating the dependencies of the eigenfrequencies at small lattice constants still suggest small gaps at $a = 800$ nm. For this lattice period we are not able to resolve the forbidden frequency gaps directly as discussed above. From Fig. 3 it is clear that in particular nanopatterning on the 100-nm length scale is key to obtain significant forbidden frequency gaps in the antidot lattices. This can be realized by direct focused ion beam patterning.²⁵

It is now interesting to explore the dispersion $f(k)$ for the diagonal direction, that is, the ΓK direction [inset of Fig. 3(a)] where \mathbf{k} is under an angle of 45° with respect to the x or y direction. To exploit periodic boundary conditions in this configuration we construct a conventional unit cell having an effective periodicity $c = a \cdot \sqrt{2}$ along the considered stripe. This is a centered lattice structure. In Fig. 2(d) we show the simulated dispersion relations for a square antidot lattice having a lattice period of 240 nm. We find a stop band near 10 GHz with a width of 0.6 GHz at the first BZ boundary with the corresponding wave vector of $k_{\text{BZb}} = \sqrt{2} \cdot \pi/a$. This forbidden frequency gap overlaps in frequency with the stop band seen in Fig. 2(c). In Fig. 3(b) we summarize extracted band edges for two different lattice periods which we simulated (i.e., 180 and 240 nm). For $a = 180$ nm we find a forbidden frequency gap near 12 GHz with a width of 1.4 GHz at the first BZ boundary. The data show that ADLs exhibit a complete stop band in the frequency range between 9.8 and 10.1 GHz for $a = 240$ nm and between 12.1 and 13.5 GHz for $a = 180$ nm.

III. DISCUSSION

In addition to the above findings we observe additional branches in the simulations for \mathbf{k} being under 45° to the x direction. An additional branch starts at 8.6 GHz at a wave vector $k = \pi/\sqrt{2}a$ and is periodic in reciprocal space. This branch does not create an avoided crossing at $k = \frac{1}{2}\sqrt{2}\pi/a = \pi/\sqrt{2}a$. In the following we explain the appearance of the additional branches in Fig. 2(d) using Fig. 4.³⁹ First we take a look at the simple cubic lattice in real space [Fig. 4(a)] and construct the corresponding lattice vectors a_1 and a_2 which define our primitive unit cell that was used for the simulation. From this we construct the corresponding reciprocal lattice [Fig. 4(b)] with the lattice vectors $|b_1| = 2\pi/a$ and $|b_2| = 2\pi/a$. The wave vector at the first BZ boundary is $k_{\text{BZb}} = b_1/2 = \pi/a$. The situation changes when we construct the reciprocal lattice from a conventional unit cell as shown in Fig. 4(c). This is relevant for our simulations with \mathbf{k} being under 45° . In this case one gets additional lattice points in the reciprocal space and the reciprocal lattice vectors b'_1 and b'_2 are different from b_1 and b_2 . It turns out that b'_1 is exactly half the size of b_3 defined in Fig. 4(b), which means we should expect an additional branch at $k_{\text{BZb}} = \sqrt{2} \cdot \pi/2a$, which we indeed see in the dispersion data [Fig. 2(d)]. The fact that we use a conventional unit cell for the simulations under 45° to apply periodic boundary conditions leads to additional reflexes in the reciprocal space. This shows that the choice of unit cell is a crucial point when simulating magnonic crystals with micromagnetic codes applying periodic boundary conditions. A careful analysis in reciprocal space is required. We note that the additional lattice points seen in the simulations

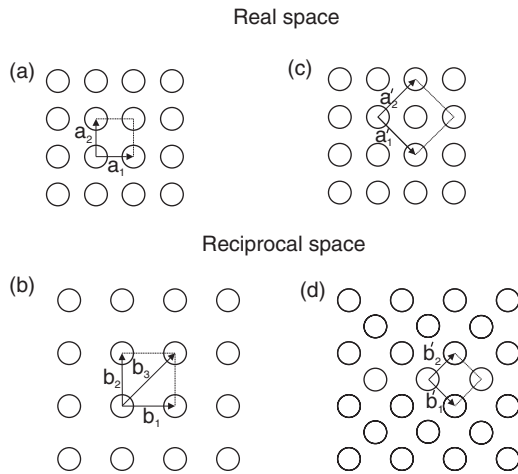


FIG. 4. Illustration of the relation between the simulated unit cells and the reciprocal lattice. We assume (a) a primitive unit cell for \mathbf{k} parallel to the ΓM direction and (c) a conventional unit cell for \mathbf{k} parallel to the ΓK direction. In (b) and (d) we show the corresponding reciprocal lattices and lattice vectors. In (d) shorter reciprocal-lattice vectors exist giving rise to additional features in the spin-wave dispersion relations (see text).

do not change the physical situation of the stop bands and corresponding branches will not be observed in an experiment.

Recent results obtained on one-dimensional MCs suggest the coherence length or dipolar coupling length of spin waves to be decisive for modeling backfolded branches in one dimension (1D) quantitatively.⁷ Correspondingly, we have used a phenomenological approach and considered an exponential fitting function to model the lattice-parameter dependencies of eigenfrequencies in Fig. 3. Due to the long-range dipolar coupling of spin excitations and possible spin-wave tunneling through the air holes⁴⁰ the miniband formation and forbidden frequency gaps are not exclusively determined by the Bragg reflection in a periodic potential. Microscopic mechanisms becoming relevant for band structure engineering are partly different from the photonic crystals. Micromagnetic

simulations generically consider all these mechanisms. But the exact analytical function for describing the data in Fig. 3 still needs to be developed. In photonics and electronics different Bravais lattices have given rise to different band structures.⁹ They are decisive for widths of the allowed bands and band gaps. In magnonics it is now interesting to explore different lattice symmetries to further optimize the artificial crystals based on spin waves. For this, micromagnetic simulations need to be further developed and optimized to simulate the translational invariance in nonsquared lattices in an efficient manner. Optimized micromagnetic codes might then allow one to study in detail tailored nonperiodic defects in MCs to further manipulate the spin wave flow. To promote further developments in magnonic crystals, design rules need to be established for the widths of both allowed minibands and complete band gaps in a perpendicular field, as was recently done for an MC in an in-plane magnetic field.²⁶

IV. CONCLUSION

In conclusion, we have shown how to create a complete stop band in a 2D magnonic crystal consisting of periodic holes in permalloy. To achieve this both nanotechnology and a perpendicular magnetic field beyond the demagnetization field of the magnetic film are important. The approach outlined here is expected to be key to guide, manipulate, and potentially trap spin waves in future magnonic devices by artificially introduced point and line defects in otherwise periodic hole lattices. Such configurations have already been powerful to tailor the flow of electromagnetic waves in photonic crystals.

ACKNOWLEDGMENTS

The authors thank Dima Berkov, Sebastian Neusser, and Florian Brandl for fruitful discussions. Financial support by the German Excellence Cluster Nanosystems Initiative Munich (NIM) and the European Community's Seventh Framework Programme (FP7/2007-2013) under Grant No. 228673 MAGNONICS is gratefully acknowledged.

*grundler@ph.tum.de

¹The sections “Emerging research materials” and “Emerging research devices” of the International Technology Roadmap for Semiconductors 2011 address spin wave devices that might be suitable for special purpose computing such as cryptography, image processing, and inference engines.

²A. Khitun, M. Bao, and K. L. Wang, *J. Phys. D: Appl. Phys.* **43**, 264005 (2010).

³S. Neusser and D. Grundler, *Adv. Mater.* **21**, 2927 (2009).

⁴V. V. Kruglyak, S. O. Demokritov, and D. Grundler, *J. Phys. D: Appl. Phys.* **43**, 264001 (2010).

⁵C. Campbell, *Surface Acoustic Wave Devices for Mobile and Wireless Communications* (Academic, New York, 1998).

⁶F. Giesen, J. Podbielski, T. Korn, M. Steiner, A. van Staa, and D. Grundler, *Appl. Phys. Lett.* **86**, 112510 (2005).

⁷J. Topp, D. Heitmann, M. P. Kostylev, and D. Grundler, *Phys. Rev. Lett.* **104**, 207205 (2010).

⁸Y. V. Gulyaev, S. A. Nikitov, L. V. Zhivotovskii, A. A. Klimov, P. Tailhades, L. Presmanes, C. Bonningue, C. Tsai, S. L. Vyotskii, and Y. A. Filimonov, *JETP Lett.* **77**, 567 (2003).

⁹J. D. Joannopoulos, S. G. Johnson, J. N. Winn, and R. D. Meade, *Photonic Crystals: Molding the Flow of Light*, 2nd ed. (Princeton University Press, Princeton, NJ, 2008).

¹⁰I. Guedes, N. J. Zaluzec, M. Grimsditch, C. Metlushko, P. Vavassori, B. Ilic, P. Neuzil, and R. Kumar, *Phys. Rev. B* **62**, 11719 (2000).

¹¹C. Yu, M. J. Pechan, and G. J. Mankey, *Appl. Phys. Lett.* **83**, 3948 (2003).

¹²C. Yu, M. J. Pechan, W. A. Burgei, and G. J. Mankey, *J. Appl. Phys.* **95**, 6648 (2004).

¹³S. McPhail, C. M. Gürtler, J. M. Shilton, N. J. Curson, and J. A. C. Bland, *Phys. Rev. B* **72**, 094414 (2005).

- ¹⁴M. J. Pechan, C. Yu, R. L. Compton, J. P. Park, and P. A. Crowell, *J. Appl. Phys.* **97**, 10J903 (2005).
- ¹⁵M. Yu, L. Malkinski, L. Spinu, W. Zhou, and S. Whittenburg, *J. Appl. Phys.* **101**, 09F501 (2007).
- ¹⁶O. N. Martyanov, V. F. Yudanov, R. N. Lee, S. A. Nepijko, H. J. Elmers, R. Hertel, C. M. Schneider, and G. Schönhense, *Phys. Rev. B* **75**, 174429 (2007).
- ¹⁷M. Kostylev, G. Gubbiotti, G. Carlotti, G. Socino, S. Tacchi, C. Wang, N. Singh, A. O. Adeyeye, and R. L. Stamps, *J. Appl. Phys.* **103**, 07C507 (2008).
- ¹⁸S. Neusser, B. Botters, M. Becherer, D. Schmitt-Landsiedel, and D. Grundler, *Appl. Phys. Lett.* **93**, 122501 (2008).
- ¹⁹D. H. Y. Tse, S. J. Steinmuller, T. Trypiniotis, D. Anderson, G. A. C. Jones, J. A. C. Bland, and C. H. W. Barnes, *Phys. Rev. B* **79**, 054426 (2009).
- ²⁰S. Neusser, G. Dürr, H. G. Bauer, S. Tacchi, M. Madami, G. Woltersdorf, G. Gubbiotti, C. H. Back, and D. Grundler, *Phys. Rev. Lett.* **105**, 067208 (2010).
- ²¹S. Tacchi, M. Madami, G. Gubbiotti, G. Carlotti, A. Adeyeye, S. Neusser, B. Botters, and D. Grundler, *IEEE Trans. Mag.* **46**, 172 (2010).
- ²²S. Tacchi, M. Madami, G. Gubbiotti, G. Carlotti, A. O. Adeyeye, S. Neusser, B. Botters, and D. Grundler, *IEEE Trans. Mag.* **46**, 1440 (2010).
- ²³H. Ulrichs, B. Lenk, and M. Munzenberg, *Appl. Phys. Lett.* **97**, 092506 (2010).
- ²⁴C.-L. Hu, R. Magaraggia, H.-Y. Yuan, C. S. Chang, M. Kostylev, D. Tripathy, A. O. Adeyeye, and R. L. Stamps, *Appl. Phys. Lett.* **98**, 262508 (2011).
- ²⁵S. Neusser, G. Duerr, S. Tacchi, M. Madami, M. L. Sokolovskyy, G. Gubbiotti, M. Krawczyk, and D. Grundler, *Phys. Rev. B* **84**, 094454 (2011).
- ²⁶R. Zivieri, S. Tacchi, F. Montoncello, L. Giovannini, F. Nizzoli, M. Madami, G. Gubbiotti, G. Carlotti, S. Neusser, G. Duerr, and D. Grundler, *Phys. Rev. B* **85**, 012403 (2012).
- ²⁷In the review process of our paper, Ref. 28 was published reporting experimental data obtained for a wave vector k close to the center of the Brillouin zone (i.e., $k \approx 0$). The lattice constant of the ALD was $a = 415$ nm. There, a systematic study of the formation of complete band gaps at Brillouin zone boundaries was not performed using the outlined theoretical approach. See Refs. 44 and 45 in Ref. 28 for further experiments at $k = 0$.
- ²⁸R. Bali, M. Kostylev, D. Tripathy, A. O. Adeyeye, and S. Samarin, *Phys. Rev. B* **85**, 104414 (2012).
- ²⁹V. Kruglyak and R. Hicken, *J. Magn. Magn. Mat.* **306**, 191 (2006).
- ³⁰S.-K. Kim, *J. Phys. D: Appl. Phys.* **43**, 264004 (2010).
- ³¹R. Arias and D. L. Mills, *Phys. Rev. B* **60**, 7395 (1999).
- ³²D. D. Stancil and A. Prabhakar, *Spin Waves: Theory and Applications* (Springer, New York, 2009).
- ³³K.-S. Lee, D.-S. Han, and S.-K. Kim, *Phys. Rev. Lett.* **102**, 127202 (2009).
- ³⁴A. V. Chumak, P. Pirro, A. A. Serga, M. P. Kostylev, R. L. Stamps, H. Schultheiss, K. Vogt, S. J. Hermsdoerfer, B. Laegel, A. Beck, and B. Hillebrands, *Appl. Phys. Lett.* **95**, 262508 (2009).
- ³⁵D. V. Berkov and N. L. Gorn, “MICROMAGUS, software for micromagnetic simulations,” 2010 [<http://www.micromagus.de/>].
- ³⁶V. V. Kruglyak, P. S. Keatley, A. Neudert, R. J. Hicken, J. R. Childress, and J. A. Katine, *Phys. Rev. Lett.* **104**, 027201 (2010).
- ³⁷Currently further metallic ferromagnets such as CoFeB are explored experimentally for magnonics (see, e.g., Ref. 23). We have measured about 2–3 km/s in a perpendicular field. This is a velocity similar to surface acoustic waves.
- ³⁸Finite-element modeling that uses a mesh of variable size might allow one to reduce the edge roughening of holes. However, the efficient fast Fourier transformation routines then need to be reconsidered in the numerical calculations.
- ³⁹S. Hunklinger, *Festkörperphysik*, 3rd ed., (Oldenbourg Verlag, München, 2011).
- ⁴⁰T. Schneider, A. A. Serga, A. V. Chumak, B. Hillebrands, R. L. Stamps, and M. P. Kostylev, *Europhys. Lett.* **90**, 27003 (2010).